Brain-derived exosome biomarkers of neuroinflammation and neuronal functional iron deficiency in newborns of overweight-obese mothers

[1,2]Phu V Tran*, [2,3,4]Andrew C. Harris, [1]Zia L. Maxim, [2]Manjula Munirathinam, [3]Peter Muelken, [5]Narmin Javadova, [6]Sowmya Kruttiventi, [5]Pamela J Kling, [6]Michelle L Baack, and [1,2]Michael K Georgieff.

[1]Department of Pediatrics, [2]Masonic Institute for the Developing Brain, [3]Department of Medicine, University of Minnesota, Minneapolis, MN 55455, USA

[4]Department of Medicine, Hennepin Healthcare Research Institute, Minneapolis, MN 55415, USA

[5]Department of Pediatrics, UnityPoint Health Meriter, University of Wisconsin-Madison, Madison, WI 53715, USA

[6]Department of Pediatrics, Sanford School of Medicine, University of South Dakota and Sanford Research, Sioux Falls, SD 57104, USA

Conflict of Interest: All authors declared no conflict of interest to disclose

Corresponding author:

Phu V. Tran, Ph.D.

420 Mayo, MMC391

516 Delaware St., SE

Minneapolis, MN 55455

Email: tranx271@umn.edu

ORCID: 0000-0002-4301-941X

Abstract

Maternal adiposity induces inflammation that may cause fetal neuroinflammation and brain iron deficiency, and thus neurodevelopmental risk. Currently, there is a lack of brain-specific biomarkers that identify neonates who are at risk, limiting the ability to screen and intervene early in life, when interventions may have the greatest impact on neurodevelopment. Leveraging emerging technology that purifies nanoparticles secreted from the brain into circulation, this study assessed the feasibility of quantifying inflammatory and iron markers carried within these nanoparticles to index brain inflammatory and iron status using a small volume of cord blood. Newborns of overweight-obese mothers exhibit evidence of low-level peripheral pro-inflammation with normal systemic iron status. In contrast, the brain shows anti-inflammatory responses and functional iron deficiency demonstrating that peripheral biomarkers may not accurately reflect brain processes. The discovery of quantifiable brain-derived biomarkers in blood samples serves as proof-of-concept that infants at-risk for long-term adverse health outcomes could be identified by non-invasive assays before becoming apparent later in life.

Graphical Abstract

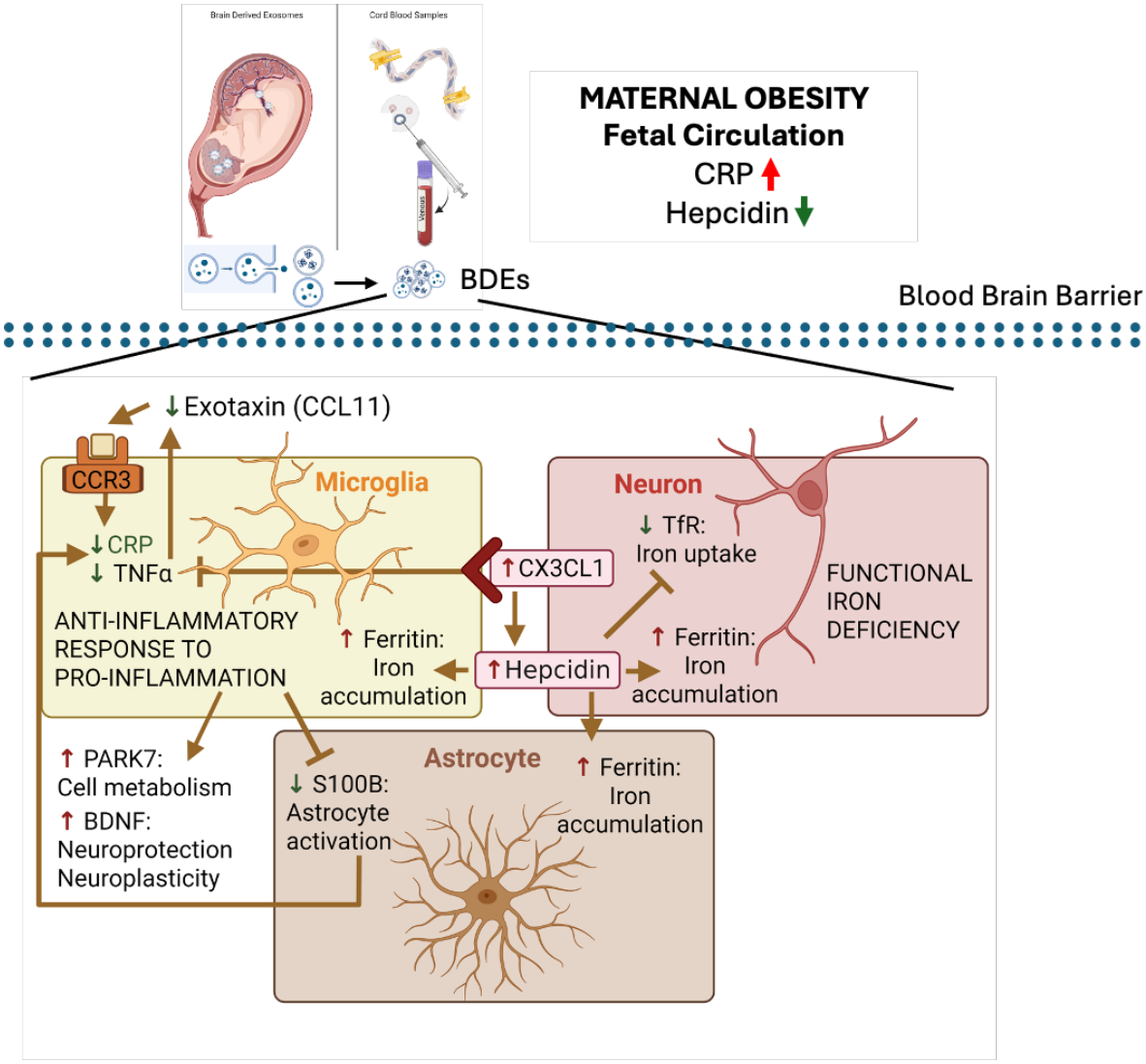

Introduction

Obesity is a risk factor for both peripheral inflammation and development of functional iron deficiency (ID) (1, 2). Emerging evidence recognizes maternal obesity as a risk factor for abnormal programming of the immune system and is associated with a higher risk of perturbed neurodevelopment in offspring (3, 4). Mechanistically, the effects of maternal obesity on neurodevelopment in the offspring in pre-clinical models have been ascribed to excess inflammatory activation (5, 6), brain iron dysregulation(7), and abnormal synaptic connectivity and neurotransmission (8, 9). However, because of barriers related to accessing the central nervous system (CNS) compartment non-invasively, no human studies have assessed the relationship between neuroinflammation (NI) and ID in neonates born to mothers with non-infectious inflammatory conditions such as excess adiposity.

Fetal neuroinflammation can directly lead to neurodevelopmental dysfunction via the inflammatory cascade's toxic effects on both gray and white matter. While CNS infection (e.g., meningitis, encephalitis) is the most severe or extreme etiology of fetal brain inflammation, a number of common neurodevelopmental disorders (NDDs), including autism spectrum disorders (ASD), attention deficit hyperactivity disorder (ADHD), and intellectual disability have been linked to less overt, non-infectious causes of NI (10-12). Emerging evidence from preclinical models and postmortem human tissue indicate that altered chemokine/cytokine signaling can lead to dysregulated cellular homeostasis (e.g., oxidative stress), reduced cell survival, and impaired neuronal differentiation (e.g., myelination, gliosis); these molecular and cellular changes are potential mechanisms underlying the link between NI and NDDs (13, 14). Extensive studies in both clinical and pre-clinical models reveal that common gestational exposures (e.g., stress, toxins, nutritional deficits, obesity, gestational weight gain) instigate metabolic derangements and

a proinflammatory state during pregnancy to perturb neurodevelopment in the developing offspring (4, 15, 16). Specifically, the status of maternal inflammation plays a critical role in programming the fetal brain immune responses, which regulate normal fetal brain development and neuronal maintenance throughout life (15). NI falls within the Developmental Origins of Health and Disease (DOHaD) concept, where early-life environment plays a major determining factor for physical and mental health across the lifespan (17).

In addition, an important link for the maintenance of physiological homeostasis is the inflammatory regulation of the systemic iron pool. Inflammation dysregulates systemic iron trafficking by increasing liver hepcidin expression and causing a functional iron deficiency anemia (18, 19). Since iron is prioritized to red cells over the brain in the fetus and neonate (20), the brain has been hypothesized to also be at risk for functional iron deficiency during pro-inflammatory states. It is unknown whether hepcidin-driven sequestration of systemic iron reduces the iron pool necessary for proper brain growth during early development (21). Maternal stress, which increases systemic high-sensitivity CRP levels, lowers iron availability in the offspring (22-24). Coe and colleagues noted a link between maternal (non-infectious) stress and infant immune response and systemic functional iron deficiency anemia in non-human primates(25), which was subsequently confirmed in humans (22). We postulated that maternal stress-induced inflammatory cytokines (e.g. IL1β, IL6) activate the liver hepcidin pathway to regulate iron homeostasis (26, 27) as a mechanism underlying the link between maternal inflammation and fetal brain iron deficiency (28), although this hypothesis has not been tested.

Functional iron deficiency is a well described red blood cell physiological response to systemic inflammation (18). In the periphery, inflammation activates the liver hormone hepcidin that reduces iron absorption from the digestive tract and cellular bioactive iron pool by mobilizing them

into ferritin, iron storage protein (26, 27, 29). These physiological responses promote functional iron deficiency in cells as available bioactive iron becomes insufficient for obligated cellular activities (e.g., hemoglobinization, metabolism, energy synthesis, oxygenation), a condition termed anemia of inflammation(26, 27). Whether the brain (or any other end-organ) becomes similarly functionally iron deficient due to iron sequestration with systemic inflammation has not been assessed although the mechanisms to induce such a response are present in the CNS (30-33). In the CNS, hepcidin has been found in astrocytes and neurons of adult humans and is associated with dementia-related disease (e.g., Parkinson, Alzheimer) pathology (30, 31). Hepcidin may be mislabeled as a hepatic protein because emerging evidence suggests that inflammation induces hepcidin expression in both neuronal and non-neuronal cells to regulate iron homeostasis in neural cells and therefore can contribute iron dyshomeostasis and subsequent cellular degeneration in neuropathologies (32, 33). Likewise, iron homeostasis is also linked to neuroinflammation via the reactive oxygen species (ROS) signaling pathway (29). Neuroinflammation can therefore lead to brain dysfunction by direct damage via the inflammatory cascade or by causing a functional iron deficiency due to a lower cellular labile iron pool or both.

Biological nanoparticles such as exosomes are a class of extracellular vesicles between 40-130 nm diameter. They are secreted by virtually all cell types and carry cargo such as proteins, carbohydrates, lipids, metabolites and nucleic acids that reflect origin cell status and serve as molecules for cell-cell communication (34, 35). In particular, trafficking of ferritin and TfR by exosomes has been described previously (36, 37). Exosomes generated by the brain cross the blood brain barrier into systemic circulation and have been explored as potential carriers of biomarkers that directly index the current physiological state of the cells that release them. They have short half-lives ranging from minutes to hours (38, 39). Exosomes originated from brain (brain-derived exosomes, BDEs) can be purified from serum or plasma using the expression of

neuronal-specific proteins such as the adhesion molecule L1CAM and the glutamate receptor (40, 41), as well as the CNTN2 glycoprotein (42, 43). Specifically, brain-derived CNTN2$^+$ exosomes carry cargo that reflects physiologic changes related to neonatal hypoxic-ischemic injury, and thus may serve as a biomarker of brain pathology (42, 43).

This study investigated the feasibility of using circulating BDEs to identify NI and brain ID risks in newborns by leveraging an easily accessible umbilical cord blood, which can be obtained non-invasively from a clamped cord segment that would otherwise be discarded after birth. Umbilical cord sampling is done immediately after birth, before the onset of postnatal confounders including neonatal nutrition. Given their short half-life (38, 39), BDEs from this source may serve as an excellent predictor of concurrent maternal inflammation and iron trafficking across the placental-fetal unit. Moreover, analysis early in life represents a critical developmental time point when close follow-up and timely postnatal interventions that can have maximal impact. Here we present evidence that contents within BDEs may also be used to index NI and ID in response to other *in utero* proinflammatory states, such as high adiposity during pregnancy. Establishing BDEs as carriers of biomarkers for fetal brain health could advance human studies without using invasive methods such as lumbar puncture for an otherwise inaccessible organ. It also provides an opportunity to relate these markers to more conventionally utilized peripheral biomarkers of inflammation and iron status.

Results

Hippocampal origin of CNTN2$^+$ exosomes

To demonstrate that BDEs accurately reflect brain concentrations of the analytes, a preclinical experiment was designed to compare the correlation between CNTN2$^+$ exosomes extracted from

plasma and exosomes extracted directly from hippocampus of postnatal day 7 rats (Fig.1a). Exosomes were isolated using our protocol (Supplemental Figure 1). Assessment of paired plasma CNTN2^{+}, CNTN2-depleted (CNTN2^{dep}), and hippocampal exosomes, indicated that only CNTN2^{+} exosomes showed positive correlations with hippocampal exosomes for IL-2 and TNFα, two quantifiable cytokines in both sample origins (Fig.1b,c).

Maternal and newborn demographics

Based on the Institute of Medicine (IOM) and American College of Obstetrician and Gynecologists (ACOG) clinical guidelines (Table 1a) (44), group numbers and demographics by pre-pregnancy weight and gestational weight gain (GWG) classifications are detailed in Table 1b and 1c, respectively. Pre- and post-pregnancy weight, pre-pregnancy BMI and maternal age were significantly different between the two-group comparison with overweight-obese (OWO) participants being heavier and younger than non-obese controls (Table 1b). While there were notable individual differences with little to no weight gain in the OWO group, no overall significant difference in gestational weight gain (GWG) during pregnancy was observed between control and OWO groups (Table 1c, p=0.18).

Characteristics of human plasma brain-derived exosomes

Exosomes isolated from cord plasma using our protocol (Supplemental Figure 1a) showed particles in the range of 40 nm to 300 nm peaking around 80-90 nm as assessed by Nanoparticle Tracking Analyzer (Supplemental figure 1b). Of the control samples, 90.7% of exosomes had 80.7 nm in diameter, whereas 83.9% of OWO exosomes had 92.0 nm in diameter, indicating appropriate sizes for exosome classification (Supplemental Table 1) (35). Analysis by transmission electron microscopy (TEM) showed nanoparticles with high structural integrity (Supplemental Figure 1c). Dot blot assays confirmed positive exosome markers (i.e., CD9, CD63,

CD81) and neural-specific markers (CNTN2$^+$, NF-L) (Supplemental Figure 1d). While there was no difference in BDE concentrations or proportion of particle distributions, the average particle diameter was larger in the OWO compared to the control group, indicating a potential trafficking of more CNS contents into the periphery in OWO (vs Cntl) pregnancies (Supplemental Figure 2).

Correlations among plasma and BDE analytes

Measurable ranges, averages and standard deviations of umbilical cord plasma and BDE-carried analytes are detailed in Table 2 with p-values denoting significant differences between control and OWO samples. Compared to non-obese control, OWO samples showed significant different for the majority of quantified analytes, particularly in the BDEs. Pearson's analyses of all measured analytes from both groups showed significant correlations among the analytes in systemic plasma and BDEs, particularly among analytes within BDEs, indicating a higher sensitivity of markers carried within BDEs (Fig.2a). Significant correlations among the quantified markers include TNFα, CRP, Eotaxin, Fractalkine (CX3CL1), ferritin, TfR, S100B, and BDNF (Fig.2a). In particular, TNFα and CX3CL1 showed positive and negative relationships in plasma and BDE, respectively, indicating divergent responses between peripheral and central inflammation (Fig.2a). To assess whether group differences influence the expression of CRP and iron markers in both plasma and BDEs, regression analyses were performed for each group. Despite no overall correlation between plasma and BDEs for TfR or ferritin, when parsing samples into groups, the OWO group had significant correlations between plasma and BDEs for TfR (Fig.2e), but less significant for ferritin (Fig.2d), suggesting an increased sensitivity of BDE to correlate iron status between the periphery and the central nervous system.

Overweight and obese pregnancy alters inflammatory signatures in umbilical cord plasma

Compared to controls, umbilical cord plasma from OWO samples had higher CRP, lower hepcidin, and no change in ferritin or TfR concentrations, indicating a pro-inflammatory state that did not disrupt peripheral iron status (Table 2, Fig.3a,b). In contrast, cord plasma-derived BDE from OWO samples had higher concentrations of hepcidin and ferritin with lower concentrations of TfR, as well as a profile of cytokines and chemokines that suggests a neuronal anti-inflammatory response to OWO (Table 2). To approximate the interaction of iron markers (TfR, ferritin) in both compartments with pre-pregnancy BMI and gestational weight gain (GWG) during pregnancy, linear regression analyses were performed for these variables. The results showed no correlation among these variables (Supplemental Figure 3), suggesting that neither pre-pregnancy BMI nor GWG in this cohort was sufficient to influence the expression changes of iron regulators in the central nervous system (CNS). Likewise, correlations were determined to further assess group differences in the peripheral immune response and iron regulation. Linear regression analysis showed a positive correlation between CRP and TNFα for the Cntl group and nearly significant (P=0.06) for the OWO group (Fig.3c), suggesting a strong likelihood of no difference in CRP response to TNFα between groups. CX3CL1 showed a positive correlation with CRP only in the OWO group, indicating an increase in inflammatory response (Fig.3d). There was no correlation between Eotaxin (CCL11) and CRP (Fig.3e). Consistent with the higher plasma CRP concentration, the OWO group, but not controls, showed positive correlations between hepcidin, ferritin, and possibly TfR (P=0.06) to plasma CRP (Fig.3f,g,h).

Overweight and obese pregnancy induces anti-inflammatory and neuroprotective signatures in BDEs

In BDEs, the OWO group showed an elevated CX3CL1 concentration, but reduced concentration of TNFα, CRP, and CCL11 (Eotaxin) compared to controls (Fig.4a), indicative of an anti-

inflammatory response in the brain, potentially to the peripheral pro-inflammatory milieu. As hypothesized (45, 46), TNFα showed a negative correlation with the neuronal-derived CX3CL1 and positive correlation with the pro-inflammatory cytokine CRP and CCL11 (Fig.4c,d,e). Linear regression slopes were differed between Cntl and OWO groups for TNFα vs CX3CL1 ($F=20.6$, $P<0.001$) and Eotaxin vs TNFα ($F=16.8$, $P<0.001$), indicating disruptions of responses such as decreased TNFα sensitivity to CX3CL1 signaling and increased Eotaxin responsiveness to TNFα in the OWO group (Fig.4d,e). To further assess downstream effects of the altered levels of BDE cytokines/chemokines and iron regulators, markers for neuroprotection and neuroplasticity (BDNF (47, 48)), metabolite-mediated cell signaling (PARK7 (49, 50)), and astrocyte activity (S100B (51, 52)) were analyzed in cord plasma BDEs. Compared to controls, OWO BDEs had higher BDNF, higher PARK7, and lower S100B concentrations (Fig.4b). To define whether the lower TNFα , higher CX3CL1, or both influence the expression changes of S100B, PARK7, and BDNF in BDEs, regression analyses were performed for these variables. For TNFα, the control group showed an inverse relationship to BDNF and PARK7, and a direct correlation with S100B (Fig.4f,g,h). The OWO group showed a decrease in correlation for PARK7 with unequal regression slopes ($F=9.89$, $P=0.003$), indicating a reduced PARK7 response to TNFα (Fig.4g). With regard to CX3CL1, the control group showed a direct relationship between CX3CL1 with BDNF and PARK7, and an inverse relationship with S100B (Fig.4i,j,k). The OWO group showed lower regression slopes for PARK7 ($F=7.32$, $P=0.009$) and S100B ($F=18.2$, $P<0.001$), indicating a loss of responses to CX3CL1 signaling. Taken together, these findings suggest both TNFα and CX3CL1 modulate expression changes of BDNF, PARK7, and S100B in BDEs.

Reduced brain iron uptake and increased brain iron storage in babies born to the OWO mothers

Given that inflammation causes systemic iron sequestration and thereby functional iron deficiency, we evaluated the effect of maternal OWO on concentration of BDE hepcidin, ferritin, and TfR (Table 2). OWO BDEs had higher levels of hepcidin and ferritin, and lower levels of TfR compared to controls (Fig.5a,b,c), consistent with activation of hepcidin-mediated shuttling of labile iron into ferritin storage and lower effort to accrete iron via TfR in the OWO group. BDE hepcidin showed positive correlations with BDE CRP and TNFα only in the OWO group with significantly different linear regression slopes between groups (hepcidin vs CRP, F=10.3, P=0.002; hepcidin vs TNFα, F=4.56, P=0.04), indicating increased hepcidin sensitivity to CRP and TNFα in the OWO group (Fig.5d,e). Also, BDE hepcidin showed an inverse and a direct relationship with gestational weight gain (GWG) and BDE S100B, respectively, only in the OWO group, suggesting that gestational weight gain during pregnancy and astrocyte activity could modulate brain hepcidin expression (Supplemental Figure 4c,d).

BDE ferritin and hepcidin concentrations were inversely correlated with a loss of significance in the OWO group, indicating a less ferritin response to hepcidin signaling (Fig.5f). Conversely, the OWO group, but not the control group, showed a significant positive correlation between TfR and hepcidin, indicating an increased TfR response to hepcidin (Fig.5g). Both control and OWO groups showed positive correlations between TfR and pro-inflammatory cytokines, TNFα and CRP, with different regression slopes (TfR vs TNFα, F=9.09, P=0.004 and TfR vs CRP, F=6.23, P=0.02), suggesting that a pro-inflammatory milieu reduces neuronal iron status marked by increased TfR concentration (Fig.5h,i). Conversely, both Cntl and OWO groups showed negative correlations between BDE ferritin and pro-inflammatory cytokines (TNFα, CRP) with difference between their regression slopes for ferritin (Ferritin vs TNFa, F=8.67, P=0.005, Fig.5j,k). As expected from the coordinated regulation of ferritin and TfR by iron responsive elements on their

respective untranslated regions of mRNAs (53), an inverse correlation between BDE ferritin and BDE TfR was found in both groups with different regression slopes (F=6.50, P=0.01, fig.5l), indicating a less sensitive TfR response to ferritin in the OWO group.

Discussion

The preclinical data supported that plasma BDEs are derivable from the hippocampus, a brain region susceptible to insults from both neuroinflammation and iron-deficiency. Using a small volume (100 μL) of cord blood, we found that cord blood BDEs and their contents can serve as a non-invasive approach to approximate brain physiological status in newborns, supporting further investigation to establish the reliability and utility of BDEs as carriers of brain biomarkers. In this particular study we found that otherwise healthy infants delivered from uncomplicated pregnancies of overweight-obese (OWO) women had elevated levels of BDE anti-inflammatory chemokine CX3CL1 and neurotrophic factor BDNF and reduced levels of BDE pro-inflammatory cytokine TNFα, CRP, and Eotaxin. These differences were accompanied by elevated levels of BDE signal for the iron sequestration (i.e., hepcidin and ferritin) concomitant with reduced signal for neuronal iron accretion (i.e., TfR). The BDE ferritin and BDE TfR were inversely and directly related to BDE proinflammatory markers (TNFα, CRP, Eotaxin), respectively, and as expected inversely related to each other. Given the known pro-inflammatory state in OWO pregnancies (6, 54), we postulate that these changes reflect higher plasma CRP levels in the cord blood of OWO compared to non-obese (control) pregnancies.

Collectively, the discovery of quantifiable BDE biomarkers to index fetal NI and brain iron status in a non-invasive sample offers a new set of tools for more direct evaluation of brain status in newborn infants at risk for long-term adverse neurodevelopmental outcomes from a diverse group

of *in utero* conditions (e.g., preeclampsia, chorioamnionitis, nutritional deficiencies, teratogen exposures). Importantly, BDE contents can be measured during a critical window of neurodevelopment when postnatal interventions could have a greater impact. The data demonstrate that peripheral biomarkers may not be accurate surrogates for changes in the brain and that assumptions of neurodevelopmental risk based on peripheral biomarkers of NI or ID should be interpreted with caution.

The rising prevalence of gestational obesity, defined as either high pre-pregnancy BMI, excessive gestational weight gain or both, from +20% in 1990s to +40% in 2019 (55) raises serious concerns for long-term health risks for the offspring, including neurodevelopmental disorders (56). As such, mechanisms underlying these health risks remain understudied, particularly regarding the link between maternal obesity and neurodevelopmental disorders in the offspring (57, 58). The key limitation of these studies is that the effects of maternal obesity on offspring brain are inferred from biomarkers measured in the peripheral circulation status, which can be unreliable. This study leveraged BDEs, nanoparticles (40-130 nm) secreted and trafficked from the CNS that were purified from cord blood, to evaluate obesity-mediated differences in molecular markers (i.e., cytokines, chemokines, nerve growth factors, indices of iron status) of relevant pathophysiologic conditions associated with maternal obesity that are carried within these BDEs. Our findings uncover a complex inter-relationship between maternal obesity and offspring peripheral vs brain physiological states. The data provide evidence that newborns of OWO mothers have elevated plasma CRP, a standard biomarker of pro-inflammation in the periphery, consistent with prior findings (54), active anti-inflammatory processes in microglia, reduction of astrocyte (and oligodendrocyte) dysfunction, and promotion of neuroprotection and neuroplasticity. In addition, the newborn brain of OWO mothers has evidence of a functional neuronal iron deficiency, similar to the anemia of inflammation (18). These findings provide insight about potential mechanisms

of action (primary acting and counteracting secondary physiological responses) among neural cell types in the developing brain of newborns of obese mothers. The lower plasma hepcidin and a trend of lower plasma ferritin (P=0.06, Table 2) concentrations suggest a potential progression of peripheral ID in newborns of OWO mothers, supporting the concept that maternal obesity is a risk factor for ID in the offspring (20, 23, 59). As such, neither pre-pregnancy BMI nor GWG appears likely a direct contributor to functional neuronal ID in the OWO offspring (Supplemental Figure 3); however, pre-existing adiposity may set the stage for, albeit subtle, a pro-inflammatory milieu during gestation that impairs iron regulation and upregulates anti-inflammatory response in the developing fetal brain.

The anti-inflammatory response of the fetal/newborn brain was an unanticipated finding that illustrates the disconnect between peripheral and centrally-derived biomarkers. CX3CL1/CX3CR1 signaling represents a neuron-microglia crosstalk, where the neuronal specific chemokine CX3CL1 activates its microglial-specific cognate receptor CX3CR1 to inhibit TNFα expression, promoting anti-inflammatory and neuroprotective processes (46, 60, 61). The inverse correlation between CX3CL1 and TNFα in BDEs is consistent with the known inhibition of TNFα by CX3CL1 signaling. This correlation was less robust and non-significant in cord plasma BDEs of the OWO group, indicating a decrease in sensitivity of fetal CX3CL1 signaling during maternal obesity. This reduced sensitivity was also observed for BDE S100B, which indexes astrocyte activity and regulates microglial TNFα (52, 62), further validating the diminished sensitivity of the CNS immune response in OWO offspring. The data show the OWO offspring have a different CNS immune responsiveness compared to offspring of non-obese controls. Whether this is an adaptive response or evidence of dysregulation is unclear and requires further investigation. The changes in the concentrations of these factors carried by BDEs indicate a potential protective

molecular response characterized by activation of cellular metabolism marked by an elevated concentration of PARK7 (49, 50), neuroprotection, neuroplasticity or both as indexed by increased level of BDNF(47), and reduced adverse astrocyte activity (astrocytosis) as indicated by lower S100B levels (51). While the link between maternal obesity and the programming of peripheral inflammation in offspring has been documented (54, 63), this study provides the first documentation in human neonates that a reprogramming occurs in the brain as well.

Maternal obesity is a known risk factor for ID in the offspring (59); however, there is limited ability to study multiple burden of risk, including NI and brain ID and associated neurodevelopmental impairments in newborns (59). That is because, until this point, there have not been reliable non-invasive markers to parse out these molecular mechanisms in asymptomatic infants. Our findings of reduced TfR concomitant with elevated ferritin in BDEs provide evidence that BDEs can index the coordinated regulation of brain ferritin and TfR and that functional ID can be detected in the CNS of OWO offspring, consistent with anemia of inflammation (high ferritin, low TfR (26, 27)). We propose that these effects were driven by elevated levels of BDE hepcidin in the OWO-exposed fetal brain. Given that CX3CL1 signaling has been hypothesized to promote hepcidin synthesis in microglia and has been associated with subsequent iron accumulation in neurons (64), our observed positive correlations between BDE hepcidin and BDE CRP and TNFα (Fig.5d,e) only in the OWO offspring support this hypothesis. In addition, our data suggest that astrocyte could be another source for hepcidin synthesis in offspring of the OWO group (Supplemental Figure 4e). Taken together, our findings are consistent with the hypothesis that regulation of iron homeostasis in the CNS relies on the local environment (low BDE CRP, high BDE CX3CL1, high BDE hepcidin) in the absence of clear evidence for systemic ID as demonstrated by little to no change in plasma ferritin or TfR concentration in this cohort. These findings provide evidence for the presence of brain functional ID preceding the signatures of

peripheral functional ID, which is consistent with the principle that iron is prioritized first to the production of the red cells at the expense of brain cells (20). The inverse correlation between BDE ferritin and BDE pro-inflammatory cytokine (TNFα, CRP) might reflect a unique regulation of brain iron homeostasis. Such a pattern of ferritin response differed from that in the plasma. This is not surprising because serum ferritin is a well-known inflammatory marker as it leaks into circulation from damaged cells (65). Indeed, we also found that plasma ferritin is directly related to plasma CRP particularly in the OWO group (Fig.3g), consistent with previously reported in infants exposed to pro-inflammatory conditions (66, 67). Conversely, we found a positive correlation of TfR and CRP (and TNFα) in BDEs, particularly for OWO offspring in this study, which is consistent with its relationship observed in the periphery (68, 69). Taken together, these findings suggest that BDE TfR might be a good biomarker to index neuronal iron demand as neurons primarily utilize TfR to uptake iron. The elevated BDE TfR in this study is consistent with iron-starved neurons, which might be driven by an absence of adequate labile iron pool due to iron sequestration into ferritin. Similarly, BDE ferritin might be a good biomarker for total brain iron status.

This study has several limitations. First, samples were collected from unlabored elective cesarean deliveries and findings may be limited to that group, but this could also be considered a strength due to the alterations of cytokines in clinical chorioamnionitis. Second, newborn CSF was not collected, but this was ethically non-feasible; thus, direct correlations between contents within plasma BDE and CSF could not be established in this cohort. Third, the cross-sectional nature of the analysis could not address whether the identified changes were long-term adaptive or dysregulated responses to maternal obesity. However, strengths of this study include the large number of samples, the highly sensitive assays, and the use of both plasma and BDE chemokines

and iron proteins. Future directions could be to interpret findings within the context of maternal iron status and to study the impact of different inflammatory stimuli and CSF cytokine and iron status, which could be performed in a non-human primate model.

In conclusion, this study demonstrates the utility and sensitivity of quantifiable BDE biomarkers for neuroinflammation and brain iron status, two highly prevalent gestational conditions world-wide that have been associated with neurodevelopmental disorders in later life. This is a major breakthrough given previous reliance on either peripheral biomarkers that may not reliably index the brain physiological states or on direct invasive procedures such as spinal tap or worse direct tissue assessment. Our findings suggest a working model for the interaction of brain inflammation and iron status in OWO offspring that reveals signals of systemic pro-inflammation and progressive iron deficiency. Furthermore, altered molecular markers in the CNS indicate neuronal functional iron deficiency accompanied by reduced neuroinflammation (Fig.6). The discovery in this study is important in that it challenges the current understanding of brain iron metabolism and immune response in two respects. First, the brain relies on the local environment for the regulation of iron metabolism and trafficking rather than peripheral iron regulation during inflammation. The general principle is that peripheral inflammation of anemia deprives iron availability for trafficking to the brain, thereby inducing brain iron deficiency. This might be true with infection-induced inflammation but would not apply to a low level of peripheral inflammation that is not sufficient to disrupt systemic iron absorption and trafficking. Second, under this non-infectious condition, the brain can protect itself by mounting an anti-inflammatory milieu in response to a low level of peripheral inflammation. This stands in contrast to the commonly accepted notion that peripheral pro-inflammation would induce pro-inflammation in the CNS. The data provide groundwork for future studies to establish BDEs as clinical tools in identifying infants at risk for long-term adverse neurodevelopmental outcomes before the development of clinical signs later in life. Such studies

could either measure BDE contents directly or by relating them to more commonly assayed peripheral biomarkers of inflammation or iron status.

Methods

Isolation of hippocampal exosomes and plasma derived BDEs from a preclinical rat model

Rat (Sprague-Dawley) pups used in this study were generated by in-house breeding. Dams were kept in a conventional rodent housing facility with ad libitum access to food and water, 22°C room temperature, and 12h/12h light/dark cycle. All procedures were approved by the Hennepin Health Research Institute IACUC (protocol #22-02). Postnatal day (P)7, equivalent to human brain development in the 3rd trimester (70), iron-sufficient rat pups (N=10, 1-2 pup/sex from 4 litters) were euthanized by decapitation under isoflurane anesthesia. Trunk blood samples were collected into EDTA (50 μL 0.5M) solution and plasma was isolated by centrifugation (13,000 RPM, 10 min, room temperature, tabletop centrifuge). Plasma was transferred into a new tube and stored at -80C. Hippocampi were micro-dissected, flash-frozen in liquid nitrogen, and stored at -80C until use.

Frozen hippocampus was homogenized in 1.0 ml of cold PBS, centrifuged at 10,000 RPM (5 min), and supernatant was transferred into a new tube. 100 μL of hippocampal lysate was digested with proteinase K (1 μg/mL, 37C, 10 min) to remove protein aggregates. Following proteinase K inactivation (ice, 5 min), exosomes were isolated from the digested hippocampal lysate and paired plasma as described below.

Isolation of exosomes

Exosomes were isolated using the Exo-Spin 96 kit following manufacturer's protocol (Cell Guidance Systems, St. Louis, MO, USA). 100 μL hippocampal lysate or plasma was applied to each column and allowed to drain by gravity. Flow-through were discarded and excess droplets removed from the column's nozzle before placing it on top of a hydrophobic collection plate. 200 μL PBS was added to each column to elute exosomes by gravity. The eluted exosomes in each well were then transferred to clean, labeled 1.5 mL tubes.

Enrichment of brain-derived exosomes (BDEs)

Brain-derived exosomes (BDEs) were enriched from total exosome preparation by immunoprecipitation (IP) using antibodies targeting CNTN2 as following: isolated plasma exosomes were incubated in polyclonal rabbit anti-CNTN2 antibody (1.0 μg optimized by titration assays assessing IP efficacy with 0.5, 1.0, 2.0, and 5.0 μg, Cat# PA5-101541, ThermoFisher Scientific, Carlsbad, CA, USA) in PBS with end-over-end rotation at 4C overnight. 100 μL protein-A Agarose beads (50% slurry, Sigma) was added into a new 1.5 microfuge tube and centrifuged for 1 min (13,000 rpm) and the liquid was removed. Exosome and antibody reaction was transferred into the tube with protein-A agarose beads and mixed for 2 hours, centrifuged 3 min (6,000 rpm). The supernatant (CNTN2-depleted fraction) was removed and stored in a new 1.5 mL tube. The exosomes/antibody/beads were then rinsed 3x with 500 μL IP wash buffer (25mM Tris-HCl pH 7.4, 150mM NaCl, 1mM EDTA, 1% NP-40, 5% glycerol), centrifuged (3 min, 6000 rpm), and discarded supernatant. BDEs were eluted with 100 μL low pH elution buffer (IgG Elution Buffer, Cat. # 21004, ThermoFisher Scientific), 2x with a 5-minute incubation time before centrifugation (2 min, 6000 rpm). 10 μL 1M TRIS pH 9.0 was added to neutralize the eluent.

Quality assessment of BDEs by nanoparticle tracker (NTA)

The quality of isolated BDEs was assessed for concentrations and sizes using a nanoparticle tracker. 10 μL exosome suspension was diluted (1:100) in milli-Q water, injected into the flow-cell using a 1 mL syringe (Norm-Ject-F Luer Solo, Air-Tite Products Inc, Virginia Beach, VA, USA), and scored by ZetaView (ZetaView QUATT, Particle Matrix, Ammersee, Germany).

Validation of BDEs by dot blots

For dot blots, 5 μL of random BDEs were assayed for exosome markers (CD9, CD63, CD81, rabbit polyclonal, Invitrogen Inc., Carlsbad, CA, USA) and neural-specific markers, including NF-L (Rabbit monoclonal, Novus Biologicals, Centennial, CO, USA) and CNTN2 (Rabbit polyclonal, ThermoFisher Scientific). Paired samples of plasma, total exosomes, and CNTN2-positive exosomes were dotted onto nitrocellulose paper. Blots were incubated in 6 mL of blocking buffer for near IR fluorescent imaging (Rockland, Pottstown, PA, USA) for 1 hour and then replaced with primary antibody (1:20,000 diluted in blocking buffer), and incubated at 4C overnight. Blots were then washed with PBS + 0.1% Tween20 (PBST) 3x and incubated in fluorescent-conjugated secondary antibody (A700, goat anti-rabbit IgG, 1:12,500 dilution) in blocking buffer for 45 minutes at RT. Blots were washed with PBST (3x) and scanned using a Li-Cor Odyssey XF instrument (Licor-bio, Lincoln, NE, USA).

Validation of BDEs by Transmission Electron Microscopy

Three random plasma BDE samples were imaged using TEM. In brief, BDE isolates (100 μL) were delivered to the Characterization Facility at the University of Minnesota for TEM imaging. TEM images were captured by negative staining samples with 1% Uranyl Acetate (UA) on glow discharged 400 mesh carbon coated Cu grids and imaging with FEI Tecnai Spirit Bio-Twin TEM at 120kV (Hillsboro, OR, USA).

Assays for quantifiable cytokines, chemokines, and iron protein markers associated with BDEs and paired hippocampal tissue exosomes of P7 rat pups

Samples were assessed by the Cytokine Reference Laboratory (CRL, University of Minnesota) using commercially available kit/reagents. This is a CLIA'88 licensed facility (license #24D0931212). Rat hippocampal exosomes (10^9 particles) and paired plasma BDEs (10^9 particles) were analyzed using the rat cytokine panel, which consists of 27-analytes (Milliplex, Millipore, St. Louis, MO, USA). Following the preparation of all reagents, samples, and standards, 50 μL of standard or sample was added to each well in duplicates. 50 μL of diluted microparticle cocktail (fluorescent color-coded beads coated with a specific capture antibody) was added to each well. The samples were incubated for 2 hours at room temperature (RT) on a shaker at 800 rpm. After removing the liquid from each well, reactions were rinsed with 100 μL Wash buffer (3x). 50 μL diluted Biotin-Antibody cocktail was then added to each well and incubated for 1 hour at RT on the shaker (800 rpm). The samples were then rinsed with 100 μL Wash buffer (3x), replaced with 50 μL diluted Strepavidin-PE, and incubated for 30 min at RT with shaking (800 rpm). Following the removal of liquid, 100 μL Wash buffer was added to the samples and signals were read using the xMAP INTELLIFLEX (R&D Systems, Minneapolis, MN, USA) instrument equipped with a dual-spectra laser, which detects the color-coded beads (analytes) and PE signals (concentration of analytes). Concentration of analytes was determined by extrapolation from 4- or 5-parameter fitted standard curves using Belysa Immunoassay Curve-Fitting software (R&D Systems).

Human subjects and biospecimen collection

Biobanked umbilical cord plasma samples used for this study were initially collected between November 2017 and February 2024 following routine cesarean section delivery of consenting pregnant participants who were enrolled in Sanford Health's Cord Blood Feasibility study (IRB

STUDY00000571: Cord Blood/Tissue Feasibility and Placenta Research). The study was carried out under guidance from Sanford's Institutional Review Board in accordance with The Federal Regulatory Guidelines (Federal Register Vol. 46, No. 17, January 27, 1891, Part 56) and guidance from the Office of Human Research Protection (45 CFR 46) as described in the 21 CFR 50, Protection of Human Subjects. Pregnancy data were collected from electronic medical records in accordance with U.S. federal Health Insurance Portability and Accountability Act (HIPAA) assurances. Consenting donors between the ages of 18-45 who were pregnant and scheduled for a planned C-section delivery at Sanford Health were included in the study. Subjects with known HIV/AIDs, Hepatitis B, Hepatitis C or other blood borne infectious diseases, those whose delivering physician felt collection of the cord blood, tissue or placenta would affect the health of the mother or infant, or those who, in the judgment of the investigator, were unable to give an informed consent for reasons of incapacity, immaturity, adverse personal circumstances or lack of autonomy were excluded from the study.

Overall, the Cord Blood Feasibility Study enrolled 300 maternal donors. This study used a subset of samples from healthy women with singleton pregnancies and no diagnosis of chorioamnionitis, diabetic pregnancy (Type 1, 2 or gestational), multiple fetal anomalies or abnormal genetic testing. Demographics data collected included maternal age, gravidity, parity, pre-pregnancy and post-pregnancy height, weight and BMI. When there was no recent pre-pregnancy weight recorded, a first-visit, first-trimester weight was substituted. Additional data collected included smoking status, pregnancy complications (including preeclampsia and diabetes), newborn gestational age, birth weight and sex. Pregnancies complicated with preeclampsia and diabetes were also excluded from the study.

For group comparisons, pre-pregnancy (or first-visit) BMI was used to cluster participants in underweight (BMI<18.5), normal weight (BMI=18.5-24.9), overweight (BMI=25-29.9) and obese (BMI≥30) categories according to the Institute of Medicine (IOM) and American College of Obstetricians and Gynecologists (ACOG) Clinical Guideline number 548 (Table 1a) (44). Women who were underweight (n=1) or normal weight (n=21) were clustered with the control group. Women who were overweight (n=14) or obese (n=24) were clustered with the overweight-obese (OWO) group. Immediately after the delivery of the infant and clamping of the umbilical cord, whole blood was collected using aseptic technique into a sterile anti-coagulant coated blood tube or sterile blood collection bag. Cord blood was refrigerated and processed by centrifugation for plasma collection as soon as feasible and always within 12 hours. Plasma was frozen and banked at -80C until use.

Quantification of cytokines/chemokines, iron markers, and hepcidin in human plasma

An aliquot (10 μL) of umbilical cord plasma was assayed for concentration of CRP, TNFα, Fractalkine (CX3CL1), Eotaxin (CCL11), BDNF, PARK7, Ferritin, S100B, and TfR performed by the Cytokine Lab using a customized panel of analytes (R&D Systems) for the Luminex platform as described above.

For hepcidin quantification, dot (array) plots were performed. Following the validation of the human hepcidin antibody for antigen specificity by western blot (Supplemental Figure 4a), plasma (4 μL of 1/10 dilution in protein lysis buffer) were dotted onto a nitrocellulose membrane using a 96-well grid. Blots were blocked in 6 mL of blocking buffer for near IR fluorescent imaging (Rockland) for 1 hour and then replaced with anti-hepcidin antibody (rabbit polyclonal antibody, 1:20,000 dilution, R&D Systems) in blocking buffer, and incubated at 4C overnight. Blots were washed with PBST (3x) and incubated in fluorescent-conjugated secondary antibody (A700, goat

anti-rabbit IgG, 1:12,500 dilution) in blocking buffer for 45 minutes at RT. Blots were washed with PBST (3x) and scanned using a Li-Cor Odyssey XF (Licor-bio, Lincoln, NE, USA) instrument. Fluorescent intensity unit (FU) for individual dot was quantified using Image Studio software (v5.2, Licor-bio) and normalized to the total volume (μL).

Quantification of analytes (chemokines, cytokines, iron protein markers, hepcidin) in human BDEs

BDEs ($1x10^9$ particles) from human umbilical cord plasma samples were first screened for quantifiable analytes using the human cytokine/chemokine/growth factor panel A, which has 48 analytes (HCYTA-60K-PXPK48, Milliplex, Millipore) and custom-designed panel consisting of cytokine (CRP), growth factor (BDNF, GDNF), cell metabolism marker (PARK7), marker for astrocyte activity (S100B), and iron marker (Ferritin, TfR). Subsequently, BDEs ($1.1x10^9$ particles) were assayed using a customized panel with CRP, TNFα, Fractalkine (CX3CL1), Eotaxin (CCL11), BDNF, PARK7, Ferritin, S100B, and TfR (R&D Systems) using the Luminex platform (xMAP INTELLIFLEX) and magnetic bead set (Cat# LXASHM-09) following manufacturer's protocol (R&D Systems) as described above.

For hepcidin quantification, 4 μL of BDE isolates were dotted onto a nitrocellulose membrane using a 96-well grid and processed as described above. BDE concentrations (particles/mL) were determined using the nanoparticle analyzer (ZetaView). Signal intensity (FU) was normalized to particle concentration in 4 μL and computed for 10^9 particles.

Sex as a biological variable

Given its proof-of-concept nature, this study was not powered to consider sex as a biological variable. Both sexes were included in all analyses.

Statistical methods

Pearson's correlation matrix was generated for continuous variables of combined plasma and BDE data. The correlation matrix was graphed using MS Excel with significant values highlighted. Simple linear regression and analysis for unequal slopes were used to determine the correlation between variables and groups. Group comparisons were made by *t*-test (OWO vs. Controls) for continuous variables, Fisher's exact test for categorical variables (e.g., smoker vs non-smoker, newborn sex), and), Brown-Forsythe and Welch ANOVA tests (to account for unequal standard deviation). Whenever the ad hoc F-test showed significant variation (unequal variance) between groups, a non-parametric *t*-test (Mann-Whitney U test) was used in place of the parametric students *t*-test. Data analyses were done using Prism (GraphPad v10). Significance was defined as $p<0.05$.

Author contributions

PVT, PJK, and MKG developed the concept and designed the study; ACH and PM generated preclinical biospecimens; NJ and PJK provided human biospecimens for the initial pilot assays (data not shown); MLB and SK provided human biospecimens of the studied cohort; MM and ZM conducted the experiments; PVT and MLB analyzed the data; PVT drafted the manuscript; PVT, PJK, MKG, and MLB reviewed and edited the manuscript; all authors reviewed and approved the manuscript.

Acknowledgements

This work was supported in part by the NIH Grant to MKG and PVT (P01-046925), financial support from the Masonic Institute for Developing Brain to PVT and ACH. Financial support from the Hennepin Healthcare Research Institute to ACH. PJK and NJ were supported by the UW Department of Pediatrics, UnityPoint Health Meriter Foundation, and Gerber Foundation. MLB was support by NIH/NIGMS P20GM103620, NIH/NHLBI R01 HL160980, NIH/NGMS P30 GM154633. SK has an AAP grant that was used to support the collection of cord blood samples to measure leptin/adiponectin cytokines: American Academy of Pediatrics Resident Research Grant.

We thank Sharon Blohowiak, BS and Natalie Dosch, MD for making available biospecimens used in the initial pilot/feasibility study. We thank Dr. James Marti in Nanotechnology Lab for assisting in the use of NTA instruments. We thank Ms. Fang Zhou for imaging of exosomes by Transmission Electron Microscopy in the Characterization Facility, University of Minnesota, which receives support in part from the NSF through the MRSEC (Award Number DMR-2011401) and the NNCI (Award Number ECCS-20245124) programs. We thank Michael Ehrhardt and Dr. Angela Mortari-Panoskaltsis of the Peds Cytokine Lab for valuable advice on assays for cytokines and chemokines. We thank our enrolled patients, clinical coordinators (Hannah Kienast, RN and Emily Andersen, RN) for their consented, enrolled, and assisted in the sample collection process. We thank Dr. Michael Olin for reviewing our manuscript.

References

1. Muñoz MPS, Ramirez ZPB, Rodriguez ELM, Blandón JDR, Aguiñaga SA, Orozco CAO, et al. Transferrin Saturation, Serum Ferritin, and C-Reactive Protein vs. Serum Ferritin for an optimal Iron Deficiency Diagnosis in Candidates for Bariatric Surgery. *Obes Surg.* 2024;34(4):1174-84.
2. Careaga M, Moizé V, Flores L, Deulofeu R, Andreu A, and Vidal J. Inflammation and iron status in bariatric surgery candidates. *Surg Obes Relat Dis.* 2015;11(4):906-11.
3. Osman HC, Moreno R, Rose D, Rowland ME, Ciernia AV, and Ashwood P. Impact of maternal immune activation and sex on placental and fetal brain cytokine and gene expression profiles in a preclinical model of neurodevelopmental disorders. *J Neuroinflammation.* 2024;21(1):118.
4. Han VX, Patel S, Jones HF, and Dale RC. Maternal immune activation and neuroinflammation in human neurodevelopmental disorders. *Nat Rev Neurol.* 2021;17(9):564-79.
5. Kang SS, Kurti A, Fair DA, and Fryer JD. Dietary intervention rescues maternal obesity induced behavior deficits and neuroinflammation in offspring. *J Neuroinflammation.* 2014;11:156.
6. Dunn GA, Mitchell AJ, Selby M, Fair DA, Gustafsson HC, and Sullivan EL. Maternal diet and obesity shape offspring central and peripheral inflammatory outcomes in juvenile non-human primates. *Brain Behav Immun.* 2022;102:224-36.
7. Graf AE, Lallier SW, Waidyaratne G, Thompson MD, Tipple TE, Hester ME, et al. Maternal high fat diet exposure is associated with increased hepcidin levels, decreased

myelination, and neurobehavioral changes in male offspring. *Brain Behav Immun.* 2016;58:369-78.

8. Hasebe K, Kendig MD, and Morris MJ. Mechanisms Underlying the Cognitive and Behavioural Effects of Maternal Obesity. *Nutrients.* 2021;13(1).

9. Musillo C, Creutzberg KC, Collacchi B, Ajmone-Cat MA, De Simone R, Lepre M, et al. Bdnf-Nrf-2 crosstalk and emotional behavior are disrupted in a sex-dependent fashion in adolescent mice exposed to maternal stress or maternal obesity. *Transl Psychiatry.* 2023;13(1):399.

10. Zhang P, Omanska A, Ander BP, Gandal MJ, Stamova B, and Schumann CM. Neuron-specific transcriptomic signatures indicate neuroinflammation and altered neuronal activity in ASD temporal cortex. *Proc Natl Acad Sci U S A.* 2023;120(10):e2206758120.

11. Sciara AN, Beasley B, Crawford JD, Anderson EP, Carrasco T, Zheng S, et al. Neuroinflammatory Gene Expression Alterations in Anterior Cingulate Cortical White and Gray Matter of Males With Autism Spectrum Disorder. *Autism Res.* 2020;13(6):870-84.

12. Padilla-Valdez MM, Díaz-Iñiguez MI, Ortuño-Sahagún D, and Rojas-Mayorquín AE. Neuroinflammation in fetal alcohol spectrum disorders and related novel therapeutic approaches. *Biochim Biophys Acta Mol Basis Dis.* 2024;1870(1):166854.

13. Chan YL, Saad S, Pollock C, Oliver B, Al-Odat I, Zaky AA, et al. Impact of maternal cigarette smoke exposure on brain inflammation and oxidative stress in male mice offspring. *Sci Rep.* 2016;6:25881.

14. Hughes HK, Moreno RJ, and Ashwood P. Innate immune dysfunction and neuroinflammation in autism spectrum disorder (ASD). *Brain Behav Immun.* 2023;108:245-54.

15. Bilbo SD, Block CL, Bolton JL, Hanamsagar R, and Tran PK. Beyond infection - Maternal immune activation by environmental factors, microglial development, and relevance for autism spectrum disorders. *Exp Neurol.* 2018;299(Pt A):241-51.

16. Rose DR, Careaga M, Van de Water J, McAllister K, Bauman MD, and Ashwood P. Long-term altered immune responses following fetal priming in a non-human primate model of maternal immune activation. *Brain Behav Immun.* 2017;63:60-70.

17. O'Donnell KJ, and Meaney MJ. Fetal Origins of Mental Health: The Developmental Origins of Health and Disease Hypothesis. *Am J Psychiatry.* 2017;174(4):319-28.

18. Nemeth E, and Ganz T. Hepcidin and Iron in Health and Disease. *Annu Rev Med.* 2023;74:261-77.

19. Sangkhae V, Fisher AL, Ganz T, and Nemeth E. Iron Homeostasis During Pregnancy: Maternal, Placental, and Fetal Regulatory Mechanisms. *Annu Rev Nutr.* 2023;43:279-300.

20. Georgieff MK. Iron assessment to protect the developing brain. *Am J Clin Nutr.* 2017;106(Suppl 6):1588s-93s.

21. Osterholm EA, and Georgieff MK. Chronic inflammation and iron metabolism. *J Pediatr.* 2015;166(6):1351-7.e1.

22. Armony-Sivan R, Aviner S, Cojocaru L, Fytlovitch S, Ben-Alon D, Eliassy A, et al. Prenatal maternal stress predicts cord-blood ferritin concentration. *J Perinat Med.* 2013;41(3):259-65.

23. Campbell RK, Tamayo-Ortiz M, Cantoral A, Schnaas L, Osorio-Valencia E, Wright RJ, et al. Maternal Prenatal Psychosocial Stress and Prepregnancy BMI Associations with Fetal Iron Status. *Curr Dev Nutr.* 2020;4(2):nzaa018.

24. Zimmermann P, Antonelli MC, Sharma R, Müller A, Zelgert C, Fabre B, et al. Prenatal stress perturbs fetal iron homeostasis in a sex specific manner. *Sci Rep.* 2022;12(1):9341.

25. Coe CL, Lubach GR, and Shirtcliff EA. Maternal stress during pregnancy predisposes for iron deficiency in infant monkeys impacting innate immunity. *Pediatr Res.* 2007;61(5 Pt 1):520-4.

26. Fleming MD. The regulation of hepcidin and its effects on systemic and cellular iron metabolism. *Hematology Am Soc Hematol Educ Program.* 2008:151-8.

27. Fleming RE. Iron and inflammation: cross-talk between pathways regulating hepcidin. *J Mol Med (Berl).* 2008;86(5):491-4.

28. Reid BM, and Georgieff MK. The Interaction between Psychological Stress and Iron Status on Early-Life Neurodevelopmental Outcomes. *Nutrients.* 2023;15(17).

29. Galy B, Conrad M, and Muckenthaler M. Mechanisms controlling cellular and systemic iron homeostasis. *Nat Rev Mol Cell Biol.* 2024;25(2):133-55.

30. Raha AA, Vaishnav RA, Friedland RP, Bomford A, and Raha-Chowdhury R. The systemic iron-regulatory proteins hepcidin and ferroportin are reduced in the brain in Alzheimer's disease. *Acta Neuropathol Commun.* 2013;1:55.

31. Raha AA, Biswas A, Henderson J, Chakraborty S, Holland A, Friedland RP, et al. Interplay of Ferritin Accumulation and Ferroportin Loss in Ageing Brain: Implication for Protein Aggregation in Down Syndrome Dementia, Alzheimer's, and Parkinson's Diseases. *Int J Mol Sci.* 2022;23(3).

32. Niida-Kawaguchi M, Kakita A, Noguchi N, Kazama M, Masui K, Kato Y, et al. Soluble iron accumulation induces microglial glutamate release in the spinal cord of sporadic amyotrophic lateral sclerosis. *Neuropathology.* 2020;40(2):152-66.

33. Puy V, Darwiche W, Trudel S, Gomila C, Lony C, Puy L, et al. Predominant role of microglia in brain iron retention in Sanfilippo syndrome, a pediatric neurodegenerative disease. *Glia.* 2018;66(8):1709-23.

34. Lin J, Li J, Huang B, Liu J, Chen X, Chen XM, et al. Exosomes: novel biomarkers for clinical diagnosis. *ScientificWorldJournal.* 2015;2015:657086.

35. Abels ER, and Breakefield XO. Introduction to Extracellular Vesicles: Biogenesis, RNA Cargo Selection, Content, Release, and Uptake. *Cell Mol Neurobiol.* 2016;36(3):301-12.

36. Yanatori I, Richardson DR, Dhekne HS, Toyokuni S, and Kishi F. CD63 is regulated by iron via the IRE-IRP system and is important for ferritin secretion by extracellular vesicles. *Blood.* 2021;138(16):1490-503.

37. Mattera VS, Pereyra Gerber P, Glisoni R, Ostrowski M, Verstraeten SV, Pasquini JM, et al. Extracellular vesicles containing the transferrin receptor as nanocarriers of apotransferrin. *J Neurochem.* 2020;155(3):327-38.

38. Oraki Kohshour M, Papiol S, Delalle I, Rossner MJ, and Schulze TG. Extracellular vesicle approach to major psychiatric disorders. *Eur Arch Psychiatry Clin Neurosci.* 2023;273(6):1279-93.

39. Banks WA, Sharma P, Bullock KM, Hansen KM, Ludwig N, and Whiteside TL. Transport of Extracellular Vesicles across the Blood-Brain Barrier: Brain Pharmacokinetics and Effects of Inflammation. *Int J Mol Sci.* 2020;21(12).

40. Yousif G, Qadri S, Parray A, Akhthar N, Shuaib A, and Haik Y. Exosomes Derived Neuronal Markers: Immunoaffinity Isolation and Characterization. *Neuromolecular Med.* 2022;24(3):339-51.

41. Patterson SA, Deep G, and Brinkley TE. Detection of the receptor for advanced glycation endproducts in neuronally-derived exosomes in plasma. *Biochem Biophys Res Commun.* 2018;500(4):892-6.

42. Pineles B, Mani A, Sura L, Rossignol C, Albayram M, Weiss MD, et al. Neuronal exosome proteins: novel biomarkers for predicting neonatal response to therapeutic hypothermia. *Arch Dis Child Fetal Neonatal Ed.* 2022;107(1):60-4.

43. Darbinian N, Sparks EC, Darbinyan A, Merabova N, Tatevosian-Geller T, Calaku K, et al. Exosomal Lipid Biomarkers of Oligodendrocyte Pathology to Predict Scoliosis in Children with Cerebral Palsy. *Obstet Gynecol Res.* 2023;6(2):160-70.

44. ACOG Committee opinion no. 548: weight gain during pregnancy. *Obstet Gynecol.* 2013;121(1):210-2.

45. Rogers JT, Morganti JM, Bachstetter AD, Hudson CE, Peters MM, Grimmig BA, et al. CX3CR1 deficiency leads to impairment of hippocampal cognitive function and synaptic plasticity. *J Neurosci.* 2011;31(45):16241-50.

46. Harrison JK, Jiang Y, Chen S, Xia Y, Maciejewski D, McNamara RK, et al. Role for neuronally derived fractalkine in mediating interactions between neurons and CX3CR1-expressing microglia. *Proc Natl Acad Sci U S A.* 1998;95(18):10896-901.

47. Song M, Martinowich K, and Lee FS. BDNF at the synapse: why location matters. *Mol Psychiatry.* 2017;22(10):1370-5.

48. Nociti V, and Romozzi M. The Role of BDNF in Multiple Sclerosis Neuroinflammation. *Int J Mol Sci.* 2023;24(9).

49. Danileviciute E, Zeng N, Capelle CM, Paczia N, Gillespie MA, Kurniawan H, et al. PARK7/DJ-1 promotes pyruvate dehydrogenase activity and maintains T(reg) homeostasis during ageing. *Nat Metab.* 2022;4(5):589-607.

50. Heremans IP, Caligiore F, Gerin I, Bury M, Lutz M, Graff J, et al. Parkinson's disease protein PARK7 prevents metabolite and protein damage caused by a glycolytic metabolite. *Proc Natl Acad Sci U S A.* 2022;119(4).

51. Michetti F, D'Ambrosi N, Toesca A, Puglisi MA, Serrano A, Marchese E, et al. The S100B story: from biomarker to active factor in neural injury. *J Neurochem.* 2019;148(2):168-87.

52. Bianchi R, Kastrisianaki E, Giambanco I, and Donato R. S100B protein stimulates microglia migration via RAGE-dependent up-regulation of chemokine expression and release. *J Biol Chem.* 2011;286(9):7214-26.

53. Kato J, Kobune M, Ohkubo S, Fujikawa K, Tanaka M, Takimoto R, et al. Iron/IRP-1-dependent regulation of mRNA expression for transferrin receptor, DMT1 and ferritin during human erythroid differentiation. *Exp Hematol.* 2007;35(6):879-87.

54. Dosch NC, Guslits EF, Weber MB, Murray SE, Ha B, Coe CL, et al. Maternal Obesity Affects Inflammatory and Iron Indices in Umbilical Cord Blood. *J Pediatr.* 2016;172:20-8.

55. Kent L. MM, Eastwood KA. Global trends in prevalence of maternal overweight and obesity: A systematic review and meta-analysis of routinely collected data retrospective cohorts. *Int J Population Data Science.* 2024;9(2):1-34.

56. Edlow AG. Maternal obesity and neurodevelopmental and psychiatric disorders in offspring. *Prenat Diagn.* 2017;37(1):95-110.

57. Merabova N, Ugartemendia L, Edlow AG, Ibarra C, Darbinian N, Tatevosian G, et al. Maternal obesity: sex-specific in utero changes in fetal brain autophagy and mTOR. *Obesity (Silver Spring).* 2024;32(6):1136-43.

58. Edlow AG, Hui L, Wick HC, Fried I, and Bianchi DW. Assessing the fetal effects of maternal obesity via transcriptomic analysis of cord blood: a prospective case-control study. *Bjog.* 2016;123(2):180-9.

59. Bahr TM, Benson AE, Kling PJ, Ohls RK, Ward DM, and Christensen RD. Maternal obesity and impaired offspring neurodevelopment: could fetal iron deficiency be a pathogenic link? *J Perinatol.* 2021;41(5):1199-200.

60. Cho SH, Sun B, Zhou Y, Kauppinen TM, Halabisky B, Wes P, et al. CX3CR1 protein signaling modulates microglial activation and protects against plaque-independent cognitive deficits in a mouse model of Alzheimer disease. *J Biol Chem.* 2011;286(37):32713-22.

61. Ré DB, and Przedborski S. Fractalkine: moving from chemotaxis to neuroprotection. *Nat Neurosci.* 2006;9(7):859-61.

62. Donato R, Sorci G, Riuzzi F, Arcuri C, Bianchi R, Brozzi F, et al. S100B's double life: intracellular regulator and extracellular signal. *Biochim Biophys Acta.* 2009;1793(6):1008-22.

63. Halonen M, Lohman IC, Stern DA, Ellis WL, Rothers J, and Wright AL. Perinatal tumor necrosis factor-α production, influenced by maternal pregnancy weight gain, predicts childhood asthma. *Am J Respir Crit Care Med.* 2013;188(1):35-41.

64. Pandur E, Tamási K, Pap R, Varga E, Miseta A, and Sipos K. Fractalkine Induces Hepcidin Expression of BV-2 Microglia and Causes Iron Accumulation in SH-SY5Y Cells. *Cell Mol Neurobiol.* 2019;39(7):985-1001.

65. Kell DB, and Pretorius E. Serum ferritin is an important inflammatory disease marker, as it is mainly a leakage product from damaged cells. *Metallomics.* 2014;6(4):748-73.

66. Beard JL, Murray-Kolb LE, Rosales FJ, Solomons NW, and Angelilli ML. Interpretation of serum ferritin concentrations as indicators of total-body iron stores in survey populations: the role of biomarkers for the acute phase response. *Am J Clin Nutr.* 2006;84(6):1498-505.

67. Thurnham DI, McCabe LD, Haldar S, Wieringa FT, Northrop-Clewes CA, and McCabe GP. Adjusting plasma ferritin concentrations to remove the effects of subclinical inflammation in the assessment of iron deficiency: a meta-analysis. *Am J Clin Nutr.* 2010;92(3):546-55.

68. Günther F, Straub RH, Hartung W, Fleck M, Ehrenstein B, and Schminke L. Association of Serum Soluble Transferrin Receptor Concentration With Markers of Inflammation: Analysis of 1001 Patients From a Tertiary Rheumatology Center. *J Rheumatol.* 2024;51(3):291-6.

69. Rohner F, Namaste SM, Larson LM, Addo OY, Mei Z, Suchdev PS, et al. Adjusting soluble transferrin receptor concentrations for inflammation: Biomarkers Reflecting Inflammation and Nutritional Determinants of Anemia (BRINDA) project. *Am J Clin Nutr.* 2017;106(Suppl 1):372s-82s.

70. Workman AD, Charvet CJ, Clancy B, Darlington RB, and Finlay BL. Modeling transformations of neurodevelopmental sequences across mammalian species. *J Neurosci.* 2013;33(17):7368-83.

Figure Legends

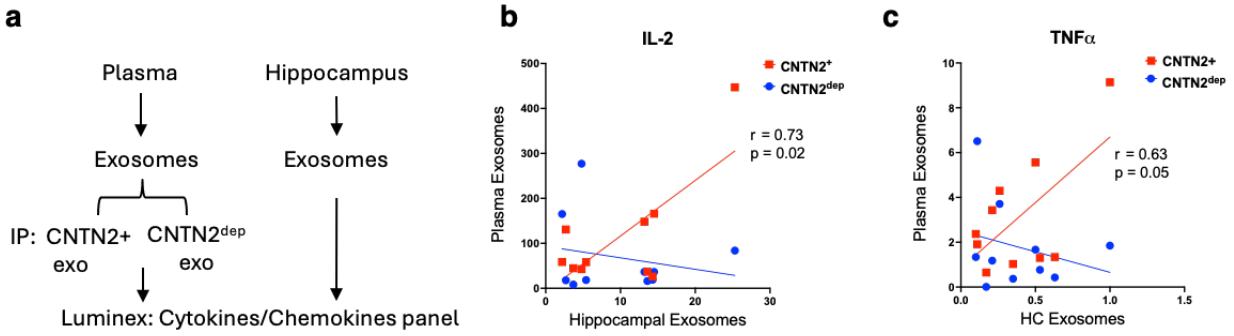

Figure 1: Validation that two cytokines in plasma BDEs correlate with hippocampal exosomes in postnatal day 7 rats. (**a**) A schematic illustrating the extraction and analysis of exosomes from plasma and hippocampus. (**b,c**) IL-2 and TNFα showed positive correlations for CNTN2^{+} (red), but not CNTN2-depleted [dep] (blue) exosomes extracted from plasma, indicating the neural origin of CNTN2^{+} exosomes. Linear regression analysis, with r coefficient and p value are shown, n=10.

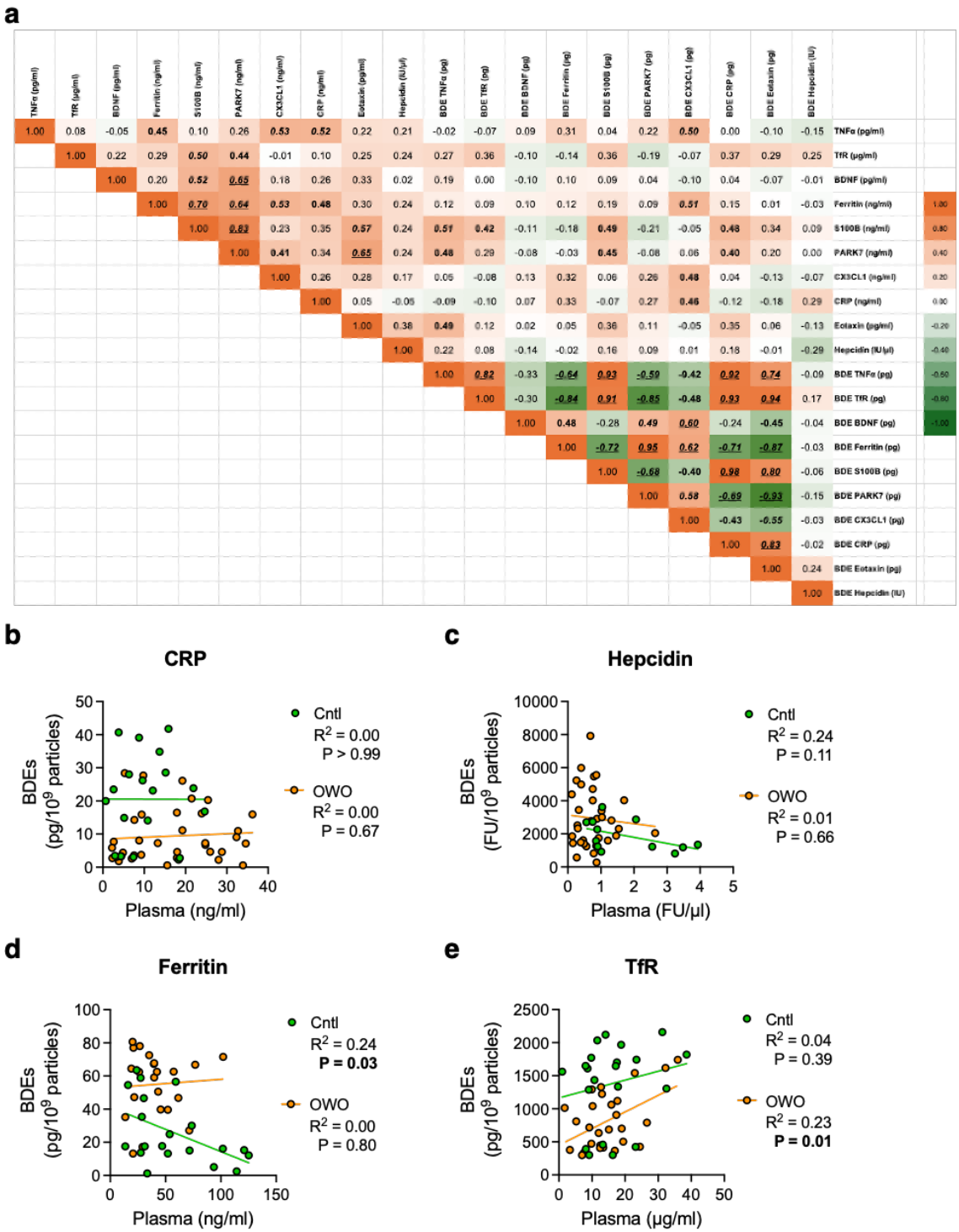

Figure 2: Comparison of quantified analytes in cord blood plasma and brain-derived exosomes. (**a**) Pearson's correlation matrix shows significant relationship among analytes. Type face denotes: Bold: P<0.05, Bold-Italic: P<0.01, and Bold-Italic-Underline: P<0.001. (**b-e**) Linear correlation plots between plasma and BDEs for CRP, hepcidin, ferritin, and TfR with parsing for non-obese control (Cntl) and overweight-obese (OWO) samples. The OWO group shows a significant correlation between BDEs and plasma for TfR.

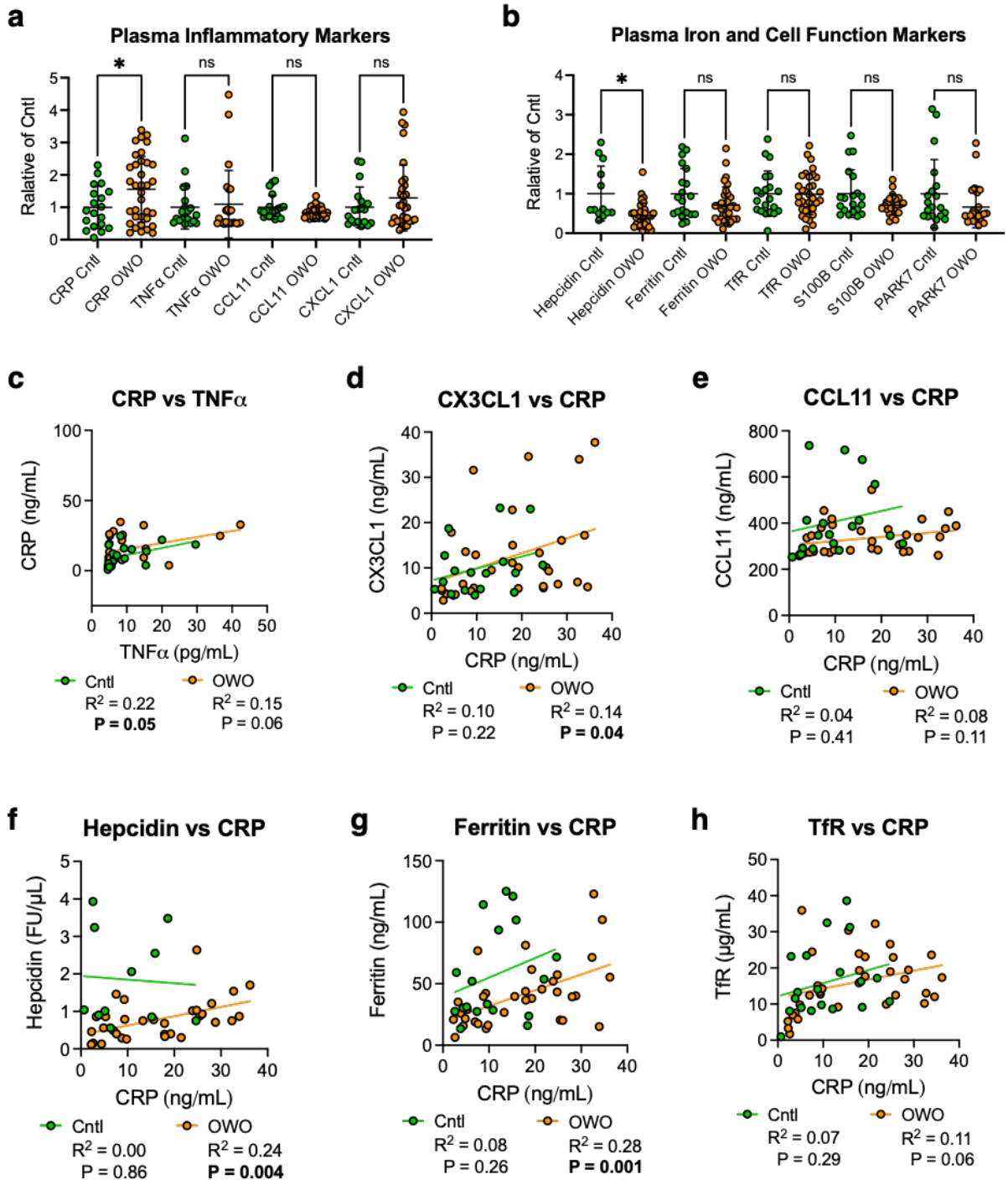

Figure 3: Changes in cord plasma markers for inflammation, iron status, and cell function. (**a,b**) Compared to non-obese control (Cntl, green), overweight-obese (OWO, orange) group showed higher CRP, lower hepcidin, and no change in ferritin or TfR concentrations. Values are Mean ± SD, n=13-21 (Cntl) and n=26-36 (OWO), Brown-Forsythe and Welch ANOVA tests, *P<0.05. (**c-h**) Linear regression analyses show direct correlations for CRP vs TNFα and for CX3CL1, hepcidin, and ferritin vs CRP only in the OWO group. Bold typeface denotes significant P-values.

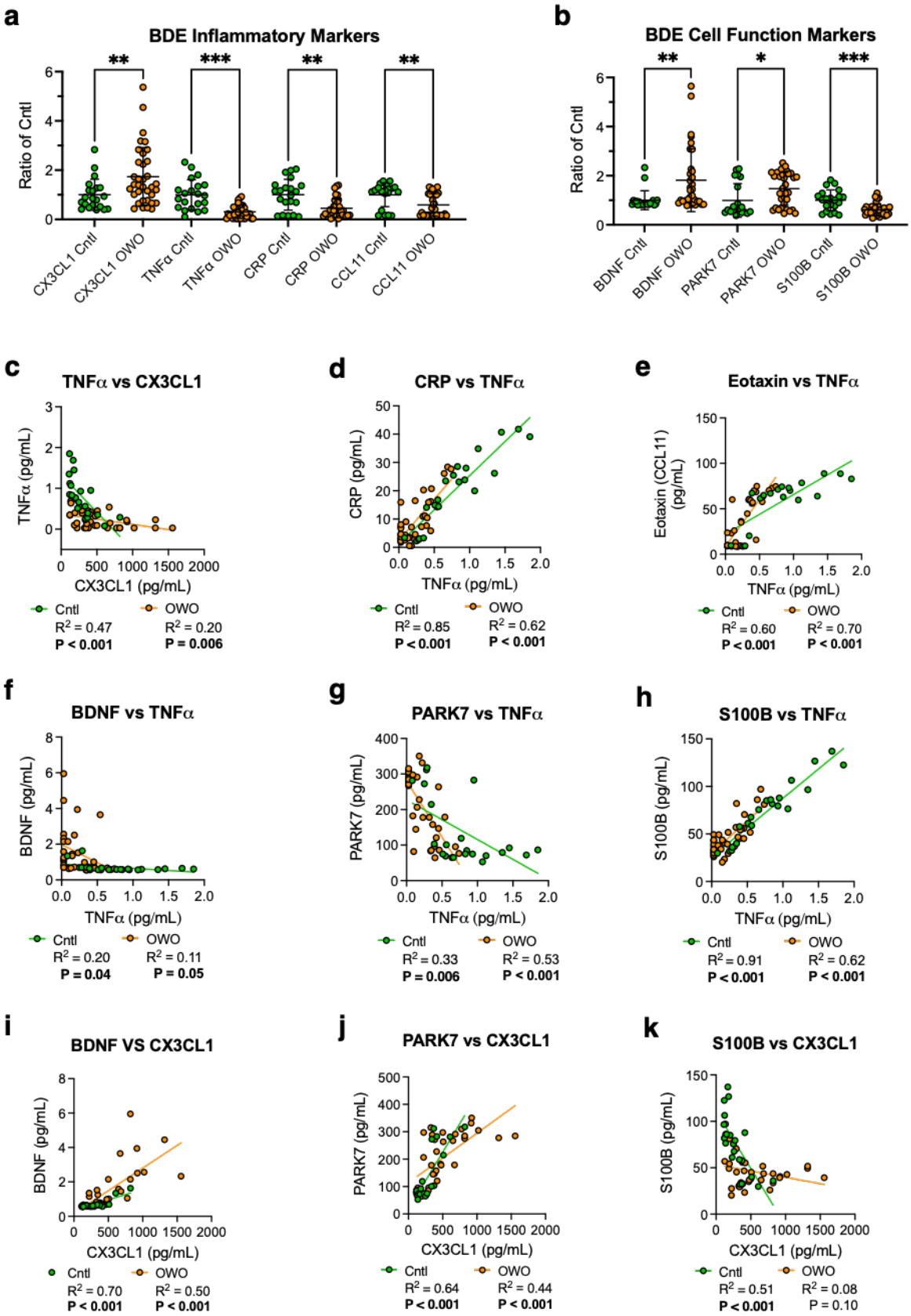
a
BDE Inflammatory Markers
Ratio of Cntl
CX3CL1 Cntl
CX3CL1 OWO
TNFα Cntl
TNFα OWO
CRP Cntl
CRP OWO
CCL11 Cntl
CCL11 OWO
b
BDE Cell Function Markers
Ratio of Cntl
BDNF Cntl
BDNF OWO
PARK7 Cntl
PARK7 OWO
S100B Cntl
S100B OWO
c
TNFα vs CX3CL1
TNFα (pg/mL)
CX3CL1 (pg/mL)
Cntl R² = 0.47 P < 0.001
OWO R² = 0.20 P = 0.006
d
CRP vs TNFα
CRP (pg/mL)
TNFα (pg/mL)
Cntl R² = 0.85 P < 0.001
OWO R² = 0.62 P < 0.001
e
Eotaxin vs TNFα
Eotaxin (CCL11) (pg/mL)
TNFα (pg/mL)
Cntl R² = 0.60 P < 0.001
OWO R² = 0.70 P < 0.001
f
BDNF vs TNFα
BDNF (pg/mL)
TNFα (pg/mL)
Cntl R² = 0.20 P = 0.04
OWO R² = 0.11 P = 0.05
g
PARK7 vs TNFα
PARK7 (pg/mL)
TNFα (pg/mL)
Cntl R² = 0.33 P = 0.006
OWO R² = 0.53 P < 0.001
h
S100B vs TNFα
S100B (pg/mL)
TNFα (pg/mL)
Cntl R² = 0.91 P < 0.001
OWO R² = 0.62 P < 0.001
i
BDNF VS CX3CL1
BDNF (pg/mL)
CX3CL1 (pg/mL)
Cntl R² = 0.70 P < 0.001
OWO R² = 0.50 P < 0.001
j
PARK7 vs CX3CL1
PARK7 (pg/mL)
CX3CL1 (pg/mL)
Cntl R² = 0.64 P < 0.001
OWO R² = 0.44 P < 0.001
k
S100B vs CX3CL1
S100B (pg/mL)
CX3CL1 (pg/mL)
Cntl R² = 0.51 P < 0.001
OWO R² = 0.08 P = 0.10

Figure 4: Changes of cytokines, chemokines, and related analytes in BDEs extracted from cord plasma immediately post birth. (**a,b**) Compared to newborns of non-obese control (Cntl, green) group, BDEs of overweight-obese (OWO, orange) group had higher CX3CL1, lower TNFα, lower CRP, lower Eotaxin (CCL11), higher BDNF, higher PARK7, and lower S100B concentrations. Values are Mean $\pm$ SD, n=21 (Cntl) and n=33-35 (OWO), Brown-Forsythe and Welch ANOVA tests, *P<0.05, **P<0.01, ***P<0.001. (**c-k**) Linear regression analyses were performed to assess the interaction between analytes. (**c,d,e**) CX3CL1 and TNFα are inversely related, whereas CRP, Eotaxin (CCL11), and TNFα are directly related. The regression slopes are significantly different between Cntl and OWO groups for TNFα vs CX3CL1 (F=20.6, P<0.001) and Eotaxin vs TNFα (F=16.6, P<0.001), indicating decreased TNFα sensitivity to CX3CL1 signaling and increased Eotaxin sensitivity to TNFα in the OWO group. (**f,g,h**) BDNF, PARK7, and TNFα are inversely related, while S100B and TNFα are directly related. The regression slopes are different between Cntl and OWO groups for PARK7 vs TNFα (F=9.89, P=0.003), indicating a decrease in PARK7 response to TNFα signaling. (**i,j,k**) For CX3CL1, BDNF and PARK7 are directly correlated, while S100B is inversely correlated with CX3CL1. Regression slopes are different between Cntl and OWO groups for PARK7 vs CX3CL1 (F=7.32, P=0.009) and S100B vs CX3CL1 (F=18.2, P<0.001), indicating a decreased sensitivity of PARK7 and S100B to CX3CL1 signaling in the OWO group. Bold typeface denotes significant P-values.

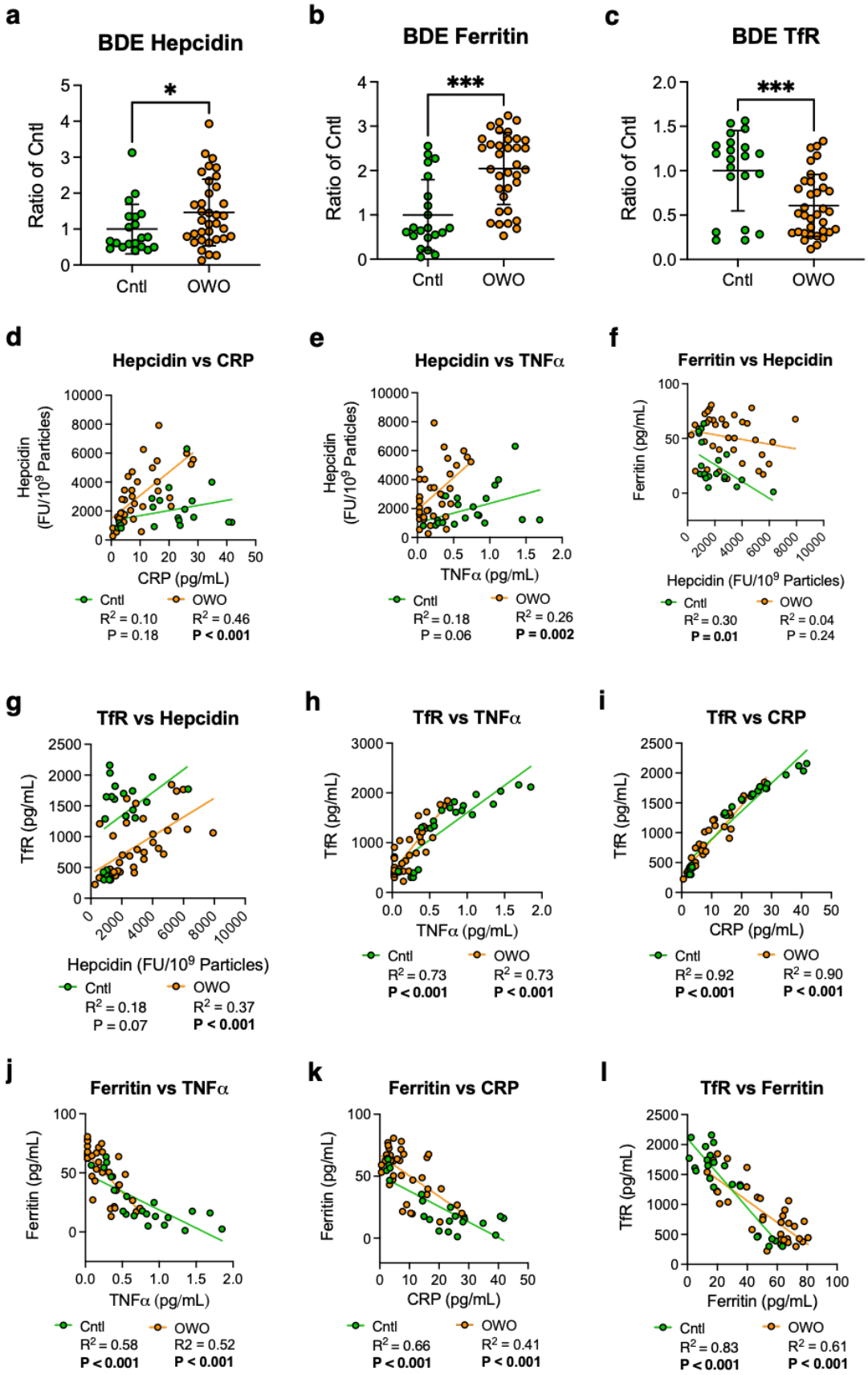
a
BDE Hepcidin
Ratio of Cntl
Cntl
OWO
b
BDE Ferritin
c
BDE TfR
d
Hepcidin vs CRP
Hepcidin (FU/10^9 Particles)
CRP (pg/mL)
Cntl R^2 = 0.10 P = 0.18
OWO R^2 = 0.46 P < 0.001
e
Hepcidin vs TNFα
TNFα (pg/mL)
Cntl R^2 = 0.18 P = 0.06
OWO R^2 = 0.26 P = 0.002
f
Ferritin vs Hepcidin
Ferritin (pg/mL)
Cntl R^2 = 0.30 P = 0.01
OWO R^2 = 0.04 P = 0.24
g
TfR vs Hepcidin
TfR (pg/mL)
Cntl R^2 = 0.18 P = 0.07
OWO R^2 = 0.37 P < 0.001
h
TfR vs TNFα
Cntl R^2 = 0.73 P < 0.001
OWO R^2 = 0.73 P < 0.001
i
TfR vs CRP
Cntl R^2 = 0.92 P < 0.001
OWO R^2 = 0.90 P < 0.001
j
Ferritin vs TNFα
Cntl R^2 = 0.58 P < 0.001
OWO R2 = 0.52 P < 0.001
k
Ferritin vs CRP
Cntl R^2 = 0.66 P < 0.001
OWO R^2 = 0.41 P < 0.001
l
TfR vs Ferritin
Cntl R^2 = 0.83 P < 0.001
OWO R^2 = 0.61 P < 0.001

Figure 5: Changes of iron indices in BDEs. (**a**,**b,c**) Compared to Cntl group, OWO group had higher hepcidin, higher ferritin, and lower TfR concentration in BDEs. Values are Mean ± SD, n=20-21 (Cntl), n=36 (OWO), *t*-test or Mann-Whitney U-test. (**d,e**) BDE hepcidin is directly related to BDE CRP and BDE TNFα only in the OWO group. Regression slopes are different between Cntl and OWO groups for hepcidin vs CRP (F=10.3, P=0.002) and hepcidin vs TNFα, (F=5.27, P=0.03), indicating increased hepcidin sensitivity to pro-inflammatory CRP and TNFα in the OWO group. (**f**) BDE ferritin is inversely related to BDE hepcidin only in the Cntl group, suggesting a decrease ferritin response to hepcidin signaling in the OWO group. (**g**) BDE TfR and BDE hepcidin show a direct correlation only in the OWO group, suggesting an increase of TfR response to hepcidin. (**h,i**) BDE TfR is directly related to TNFα and CRP with different regression slopes between Cntl and OWO groups (TfR vs TNFα, F=9.09, P=0.004; TfR vs CRP, F=5.32, P=0.03), indicating a decreased TfR response to BDE pro-inflammatory cytokines. (**j,k**) Both Cntl and OWO groups show negative correlations between ferritin and pro-inflammatory cytokines (TNFα, CRP) with a different regression slope for Ferritin vs TNFα (P=8.67, P=0.005), indicative of increased ferritin sensitivity to TNFα in the OWO group. (**l**) BDE TfR and BDE ferritin are inversely related with unequal regression slopes between Cntl and OWO groups (F=7.23, P=0.01), indicating a less sensitive TfR response to ferritin in the OWO group.

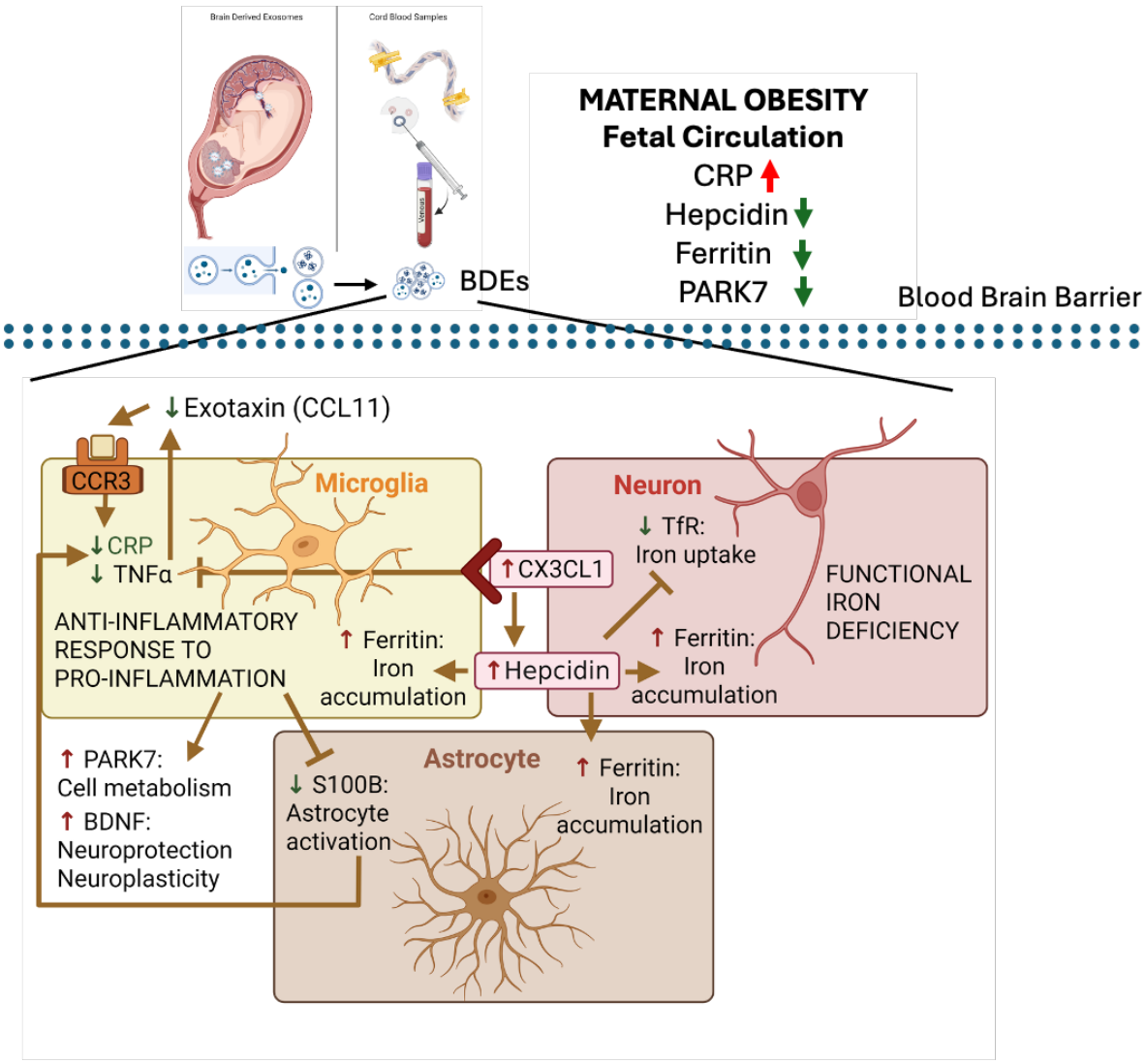

Fig.6: A proposed model of altered brain immune response and iron indices in fetuses/newborns of overweight-obese mothers through altered maternal-fetal metabolic milieu on microglia, astrocytes, and neurons. Maternal obesity can induce the cross-talks among fetal neural cells, including activation of the neuron-microglia CX3CL1/CX3CR1 signaling and astrocyte-microglia S100B signaling, leading to anti-inflammatory responses, including promotion of neuroprotection and/or neuroplasticity (via BDNF) and cell metabolism (via PARK7). Conversely, maternal obesity can induce cellular functional iron deficiency (high ferritin, low TfR), negatively affecting neural cell iron status. Hepcidin, an acute phase protein and also the master iron regulator may play a role. Image was constructed in part using BioRender software.

Tables

Table 1 - Demographic data of the studied cohorts

Table 1a. Clinical Gestational Weight Gain Guidelines Based on Pre-pregnancy BMI

Weight Category	Pre-pregnancy BMI	Inadequate GWG	Appropriate GWG	Excessive GWG
Underweight	<18.5	<12.7 kg (<28 lbs)	12.7-18.2 kg (28-40 lbs)	>18.2 kg (>40 lbs)
Normal weight	18.5-24.9	<11.4 kg (<25 lbs)	11.4-15.9 kg (25-35 lbs)	>15.9 kg (>35 lbs)
Overweight	25-29.9	<6.8 kg (<15 lbs)	6.8-11.4 kg (15-25 lbs	>11.4 kg (>25 lbs)
Obese	≥30	<5 kg (<11 lbs)	5-9.1 kg (11-20 lbs)	>9.1 kg (>11 lbs)

Body mass index (BMI), as pre-pregnancy or first trimester weight (kg) divided by height (m^2). Weight and gestational weight gain (GWG) categories are adapted from Institute of Medicine and American College of Obstetricians and Gynecologists (ACOG) guidelines, "Weight Gain During Pregnancy", Committee Opinion number 548, January 2013.

Table 1b. Demographics by Pre-pregnancy Weight Group

Demographic	Control (n=22)	OWO (n=38)	p-value
Pre-pregnancy weight (kg)	59.74 ± 6.20	90.40 ± 19.90	**<0.0001**
Pre-pregnancy BMI	22.23 ± 1.97	33.02 ± 6.75	**<0.0001**
Post-pregnancy weight (kg)	72.00 ± 7.65	99.82 ± 16.19	**<0.0001**
Gestational Weight Gain (kg)	12.20 ± 5.53	9.67 ± 7.45	0.18
Inadequate Weight Gain (%)	41%	23%	0.15*
Appropriate Weight Gain (%)	32%	22%	0.54*
Excessive Weight Gain (%)	27%	54%	0.06*
Age (yr)	31.82 ± 4.56	29.40 ± 4.19	**0.03**
Gravidity (n)	2.73 ± 1.28	3.22 ± 1.25	0.15
Parity (n)	2.23 ± 0.97	2.44 ± 1.03	0.45
Smoking (%)	9.10%	5%	0.61*
GA (weeks)	38.70 ± 0.84	38.60 ± 0.97	0.62
Birth Weight (kg)	3.34 ± 0.46	3.51 ± 0.46	0.22
Birth Weight Percentile	51 ± 31	63 ± 25	0.10

Birth Weight Z-score (n)	0.07 ± 1.01	0.45 ±0.83	0.11
Male (%)	59%	53%	0.79*

Data include mean ± standard deviation. Group differences were calculated by T-test or *Fisher's exact test. Significant p values of <0.05 are bold.

Table 1c. Demographics by Gestational Weight Gain Group

Demographic	**Inadequate (n=19)**	**Appropriate (n=15)**	**Excessive (n=26)**	**p-value**
Pre-pregnancy weight (kg)	82.70 ± 27.40	77.91 ± 20.47	77.75 ± 18.17	0.73
Pre-pregnancy BMI	31.16 ± 10.21	28.74 ± 6.92	28.18 ± 5.83	**0.04**
Post-pregnancy weight (kg)	87.32 ± 22.75	88.26 ± 17.91	93.55 ± 16.89	0.49
Gestational Weight Gain (kg)	4.42 ± 5.91	10.39 ± 4.10	15.86 ± 4.28	**<0.0001**
OWO Group (%)	50%	56%	79%	0.09
Age (yr)	30.72 ± 5.42	32.63 ± 4.56	28.89 ± 3.52	**0.03**
Gravidity (n)	3.11 ± 1.23	3.12 ± 1.36	2.86 ± 1.18	0.71
Parity (n)	2.56 ± 0.92	2.13 ± 0.62	2.29 ± 1.12	0.41
Smoking (%)	11%	0%	7%	0.47
Preeclampsia (%)	0%	6%	7%	0.61
GA (weeks)	38.75 ± 0.72	38.59 ± 1.06	38.97 ± 1.06	0.45
Birth Weight (kg)	3.33 ± 0.58	3.46 ± 0.39	3.47 ± 0.42	0.54
Birth Weight Percentile	50.78 ± 18.25	62.31 ± 23.76	61.54 ± 25.87	0.37
Birth Weight Z-score (n)	0.08 ± 1.11	0.47 ± 0.87	0.37 ± 0.79	0.42
Male (%)	50%	69%	46%	0.42

Data include mean ± standard deviation. Group differences were calculated using one-way ANOVA or *Fisher's exact test. Significant p values of <0.05 are bold.

Table 2 - Concentrations of analytes from plasma and brain-derived exosomes from cord blood

Source	Analyte	Control Mean ± SD [Range] N=13-22	OWO Mean ± SD [Range] N=25-36	*P-value
Plasma	BDNF (pg/mL)	653 ± 708 [98.0 – 2417]	302 ± 182 [105 – 818]	0.19
	CCL11 (Eotaxin) (pg/mL)	404 ± 149 [253 – 736]	334 ± 69.7 [258 – 545]	0.09
	CRP (ng/mL)	10.7 ± 6.99 [0.67 – 24.6]	16.6 ± 10.9 [2.22 – 36.2]	**0.04**
	CX3CL1 (Fractalkine) (ng/mL)	9.58 ± 6.01 [3.99 – 23.2]	12.4 ± 9.78 [2.85 – 37.7]	0.41
	Ferritin (ng/mL)	57.3 ± 36.4 [13.6 – 125]	41.0 ± 26.1 [6.46 – 123]	0.06
	Hepcidin (FU/μL)	1.71 ± 1.19 [0.56 – 3.93]	0.77 ± 0.54 [0.12 – 2.64]	**0.002**
	PARK7 (ng/mL)	19.4 ± 16.8 [2.89 – 61.0]	12.8 ± 10.1 [3.79 – 44.2]	0.11
	S100B (ng/mL)	2.47 ± 1.49 [1.07 – 6.11]	1.76 ± 0.62 [0.74 – 3.35]	0.21
	TfR (μg/mL)	16.2 ± 9.32 [0.96 – 38.6]	16.0 ± 8.30 [1.72 – 35.9]	0.94
	TNF-alpha (pg/mL)	9.47 ± 6.33 [4.60 – 29.6]	10.4 ± 9.56 [4.60 – 42.4]	0.73
BDEs	BDNF (pg/10^9 particles)	0.70 ± 0.27 [0.56 – 1.63]	1.49 ± 1.28 [0.55 – 5.95]	**<0.001**
	CCL11 (Eotaxin) (pg/10^9 particles)	56.9 ± 27.4 [8.63 – 88.8]	33.3 ± 25.8 [8.28 – 74.9]	**0.002**
	CRP (pg/10^9 particles)	20.5 ± 12.8 [2.26 – 41.8]	9.41 ± 7.76 [0.55 – 28.4]	**0.002**
	CX3CL1 (Fractalkine) (pg/10^9 particles)	290 ± 183 [113 – 822]	525 ± 365 [122 – 1557]	**0.005**
	Ferritin (pg/10^9 particles)	24.9 ± 19.8 [1.18 – 63.6]	51.3 ± 20.0 [13.2 – 80.6]	**<0.001**
	Hepcidin (FU/10^9 particles)	2016 ± 1387 [814 – 6303]	2979 ± 1855 [268 – 7924]	**0.05**
	PARK7 (pg/10^9 particles)	138 ± 94.9 [52.8 – 318]	207 ± 92.4 [64.6 – 351]	**0.01**
	S100B (pg/10^9 particles)	75.1 ± 31.6 [29.8 – 137]	46.2 ± 18.1 [20.4 – 97.1]	**<0.001**
	TfR (pg/10^9 particles)	1382 ± 626 [300 – 2160]	862 ± 467 [162 – 1845]	**<0.001**
	TNF-alpha (pg/10^9 particles)	0.80 ± 0.49 [0.08 – 1.85]	0.24 ± 0.21 [0.03 – 0.74]	**<0.001**

**t*-test or Mann-Whitney U-test. Significant P-values are in bold.